EFDA–JET–CP(12)06/04

H. Weisen, Y. Camenen, A. Salmi, M. Gelfusa, T.W. Versloot, P.C. deVries,
M. Maslov, T. Tala, M. Beurskens, C. Giroud
and JET EFDA contributors

Non-diffusive Momentum Transport in JET H-mode Regimes: Modelling and Experiment

Non-diffusive Momentum Transport in JET H-mode Regimes: Modelling and Experiment

H. Weisen[1], Y. Camenen[2], A. Salmi[3], M. Gelfusa[4], T.W. Versloot[5], P.C. deVries[5], M. Maslov[6], T. Tala[7], M. Beurskens[6], C. Giroud[6] and JET EFDA contributors*

JET-EFDA, Culham Science Centre, OX14 3DB, Abingdon, UK

[1]Centre de Recherches en Physique des Plasmas, Association EURATOM - Confédération Suisse, EPFL, 1015 Lausanne, Switzerland
[2]PIIM UMR 7345, CNRS/Aix-Marseille Univ., France
[3]Association EURATOM-Tekes, Aalto University, Finland
[4]Associazione EURATOM-ENEA-University of Rome "Tor Vergata", Roma, Italy
[5]FOM Institute Rijnhuizen, Association EURATOM-FOM, The Netherlands
[6]EURATOM-CCFE Fusion Association, Culham Science Centre, OX14 3DB, Abingdon, OXON, UK
[7]Association EURATOM-Tekes, VTT, Finland
** See annex of F. Romanelli et al, "Overview of JET Results", (24th IAEA Fusion Energy Conference, San Diego, USA (2012)).*

Preprint of Paper to be submitted for publication in Proceedings of the
24th IAEA Fusion Energy Conference (FEC2012), San Diego, USA
8th October 2012 - 13th October 2012

ABSTRACT.
A broad survey of the experimental database of neutral beam heated baseline H-modes and hybrid scenarios in the JET tokamak has established the ubiquity of non-diffusive momentum transport mechanisms in rotating plasmas. As a result of their presence, the normalised angular frequency gradient $R\nabla\omega/\omega$ is higher than expected from momentum diffusion alone, by about unity in the core (r/a~0.3), rising to near 5 close to the edge, where its contribution to the total gradient is comparable to the gradient associated with the diffusive flux. The experimental plasma parameters have been used as input for an extensive set of linear gyrokinetic simulations using GKW. The magnitude and parameter dependencies of the non-diffusive contribution to the gradient are consistent with a theoretically expected pinch, which has its origin in the vertical particle drift resulting from the Coriolis force. Linear gyrokinetic calculations of the pinch number RV/χ_ϕ and the Prandtl number χ_ϕ/χ_i, are in fair agreement with the experimental observations, with similar dependencies on R/L_n, q and $\varepsilon=r/R$ for the convective part. However, the predicted non-diffusive transport is about 30% lower, on average, than the one inferred from observation. A second round of linear gyrokinetic simulations, with more realistic assumptions, has been initiated to clarify whether the difference may be attributed to residual stresses.

1. INTRODUCTION

In recent years, substantial experimental evidence for momentum transport processes that cannot be attributed to diffusion alone has been reported from several tokamaks including JET. Extensive references can be found e.g. in [1-5]. In the JET device, evidence for an inward momentum pinch originated from neutral beam injection (NBI) modulation experiments obtained largely in fairly quiescent, low power H-modes and a few L-modes [6,7]. These findings motivated a broad based database survey destined to establish to which extent the pinch identified in those experiments was ubiquitous and in particular, if it was present in higher power, higher performance baseline H-modes and hybrid scenarios. The database constituted for this purpose covers the entire JET operating domain in baseline H-mode and hybrid scenarios and contains several hundred steady-state profiles of the relevant plasma parameters.

The local steady state momentum transport equation can be written as

$$t = -\chi_\phi l\nabla\omega/\omega + (\Gamma_N/n_i + V)l + \tau_{rs} \qquad (1)$$

Here $t = T/(dV_{FS}/dr)$ is the local torque surface density (N/m) from NBI, with $T(r)$ the volume integrated torque density, $V_{FS}(r)$ the volume of the flux surface and r the average midplane minor radius. $l=m_i n_i R^2\omega$ is the angular momentum density, m_i the average ion mass, n_i the ion density, R the average major radius of the flux surface under consideration, ω the toroidal angular velocity, Γ_N is the particle flux associated with the particle source provided by neutral beam heating, χ_ϕ is the radial momentum diffusivity, V is the momentum pinch velocity, and τ_{rs} refers to residual stress

contributions. In addition to the torque associated with NBI, torques resulting from fast ion losses and charge exchange losses may have to be considered, especially near the plasma boundary. For comparison with theory, eq.(1) is rearranged, written in dimensionless form and normalized as:

$$R\frac{\nabla\omega}{\omega} = -\frac{\chi_i}{\chi_\phi}\left\{\frac{Rt}{\chi_i I} - \frac{R\Gamma_N}{\chi_i n_i}\right\} + \frac{RV}{\chi_\phi} + \frac{R\tau_{rs}}{\chi_\phi I} \qquad (2)$$

In eq.(2), $\chi_i = Q_i/(n_i \nabla T_i)$ is the ion heat diffusivity, which is determined from the local power balance as $Q_i = Q_{iNB} + Q_{ei}$ [W/m^2], where Q_{iNB} is the ion heat flux provided by the neutral beams and Q_{ei} is the electron-ion equipartition flux. About one third of the samples included a modest fraction of hydrogen minority ion cyclotron resonance heating (ICRH), which mostly heats the electrons. Any ion heating from ICRH was neglected in this study. The normalized angular velocity gradient in eq.(2) was obtained from CXRS measurements, while the term between brackets, the normalized net dimensionless torque $t_i^* - \Gamma_N^*$, was obtained from a combination of measurements and calculations. An alternative form for eq.(2), suitable for dataset containing low values of ω is obtained by multiplying eq.(2) by $u = R\omega/v_i = R\omega/(2T_i/m_i)^{1/2}$, the Mach number. In JET NBI H-modes and hybrid scenarios, near zero rotation is only obtained near the edge in the presence of strong toroidal ripple [8]. Ripple discharges are not included in this comparison with gyrokinetical calculations in this paper, making eq.(2) the most convenient form for cross-comparison.

Table 1 shows the range of variation of the key dimensionless parameters in the database.

2. GKW linear calculations

A representative subset of >400 samples of the experimental database was used as input for a series of linear gyrokinetic calculations performed with the *δf* flux-tube code GKW [9]. This subset was selected such as to remain representative of the same dimensionless parameter domain as the entire experimental dataset. They also cover a wide radial range, expressed by the variable $\varepsilon = r/R$, with ε spanning the range *0.075* to *0.255*, the LCFS being near $\varepsilon = 0.3$. The calculations were performed for two representative wave vectors, $k_\theta \rho_i = 0.15$ & 0.45, where $k_\theta \rho_i = 0.45$, roughly corresponds to the wave vector of maximum growth rate, assuming a circular geometry, electrostatic fluctuations and two kinetic species (deuterons and electrons). In the present database, with $O_{rs} = \rho_i^*(R/L_{Ti})^2/u < 1$ for most cases, the pinch is expected to be the largest non-diffusive contribution to the momentum flux [2] and a first set of simulations was therefore performed without background E×B shear flow or other residual stress contributions. The dominant instability was identified to be the ion temperature gradient (ITG) mode. For each input parameter combination, two calculations were performed. The first of these, with $u = 0.1$ and $u' = uR/L_\omega = 0$ provided the momentum pinch part, while the second, with $u = 0$ and $u' = 1$ provided the diagonal (diffusive) part. The Prandtl and pinch numbers were then deduced from the fluxes obtained in each case as described in ref. [10]. The resulting change in momentum flux (i.e. torque t) allows a separation into a diffusive and a pinch contribution, the former being characterised by $R/L_\omega \mu t$. Collisional and non-collisional

calculations mostly produce similar results, in agreement with refs [11,12]. The choice of linear simulations is mainly dictated by practical reasons, however, it is also supported by the fact that the dominant parametric dependencies of the pinch number are largely similar in linear [13] and non-linear calculations [2]. The spectral averages for linear calculations are expected to fall between the ones for the two wavenumbers chosen.

The calculated transport coefficients, especially the pinch number RV/χ_ϕ, show a clear dependence on ε, as seen in fig.1. The horizontal bars represent the radial intervals over which the experimental gradients, which served as input for GKW, were evaluated. The horizontal bars represent the standard deviation of the calculated data for each position, reflecting dependencies on other parameters.

Since the parameter space is so vast, as well as correlated, no unique and unambiguous scaling relationship for the transport parameters can be derived. However linear regressions can help identify the most important dependencies. In figure 2 we show the best five parameter fits for the average pinch number for $k_\theta\rho_i = 0.15$ and *0.45 at a mid-radius position and nearest to the edge*. (Fits with larger numbers of parameters tend to yield at least one coefficient which is statistically insignificant or irrelevant). The regressions shown are given with their fit coefficients (b), their uncertainty δb corresponding to a 90% confidence level, the statistical significance b/δb, labeled STS, and the statistical relevance labeled STR. The latter is defined, for each parameter i, as $b_i\sigma_i/\sigma_{target}$, where σ_i is the standard deviation of parameter i and σ_{target} is the standard deviation of the target variable, here RV/χ_ϕ. The STR indicates which part of the variations of the target variable can be attributed to the variations of the regression variable.

These regressions correspond to

at $\varepsilon = 0.165$: $RV/\chi_\phi \approx 0.35R/L_n + 0.052R/L_{Te} + 0.17T_i/T_e + 0.59q + 0.36s - 1.2$ (3)

with $\sigma = 0.2$, *STS = [4.5, 1, 0.5, 5, 1.9, 2.2]* and *STR = [0.53, 0.13, 0.06, 0.69, 0.25, 0];*

at $\varepsilon = 0.255$: $RV/\chi_\phi \approx 0.45R/L_n + 0.052R/L_{Te} + 0.88T_i/T_e + 0.29q - 0.24s - 0.23$ (4)

with $\sigma = 0.32$, *STS = [11, 2, 2.8, 3.8, 3.3, 0]* and *STR = [0.88, 0.17, 0.22, 0.27, 0.26, 0].*

They identify R/L_n, q and s to be most important parameters locally, consistently with [13]. As $\varepsilon^{1/2}$, the trapped particle fraction, is also an important scaling variable [14], we provide a global regression including this parameter over all seven positions and averaged over both wavenumbers in fig.3:

$$RV/\chi_\phi \approx 0.44R/L_n + 0.077R/L_{Te} + 0.31q - 0.21s + 6.8\varepsilon^{1/2} - 2.8 \quad (5)$$

With $s = 0.31$,

STS = [*17, 4.7, 7, 4.6, 6.4, 7.3*] and *STR = [0.73, 0.16, 0.22, 0.27, 0.33, 0].*

Overall, the regressions identify R/L_n, $\varepsilon^{1/2}$, q and s as the most important scaling variables, although it should be born in mind, that the coefficients are influenced by correlations in the database. A correlation table is presented ref.[5].

3. COMPARISONS WITH EXPERIMENTAL RESULTS

The simplest way to present experimental results is by performing simple 2 parameter regressions for eq.(2) for the seven sampling positions througout the database. It can been, that despite the wide parameter range robust regression, providing typical Prandtl numbers in the range 0.75-1 and convection numbers ranging from 1 (nearest to the plasma center) to 5 (nearest to the edge) are obtained. The radial dependence of these experimental convection number is similar to the one shown for the theoretical pinch, however the experimental values are some 50% larger.

Similar momentum transport coefficients have been obtained independently from the analysis of toroidal ripple experiments, where the counter current torque caused by ion losses brought down pedestal rotation to near zero [5]. As for the GKW calculations, we can perform regressions on the experimental data. For $\varepsilon=0.165$, only two statistically significant parameters can be fitted, while for $\varepsilon = 0.255$, where the non-diffusive components are strongest, up to 5 parameters can be fitted.

The two regressions correspond to:

At $\varepsilon = 0.165$: $R/L_\omega \approx 1.1(t_i^*-\Gamma_N^*)-2.8T_i/T_e + 5.3$ (6)

With $\sigma = 0.91$, $STS = [7.3, 2.1, 3.9]$ *and* $STR = [0.72, 0.2. 0]$.

At $\varepsilon = 0.255$: $R/L_\omega \approx 1.1(t_i^*-\Gamma_N^*)+0.47R/L_n + 0.71q + 0.22R/L_{Te} -2.8T_i/T_e+2.9$ (7)

with $\sigma = 1.74$, $STS = [6.1, 2.1, 1.3,1.2,1.8, 0.9]$, $STR = [0.65, 0.23, 0.13, 0.11, 0.17, 0]$.

While for $\varepsilon= 0.165$ noise in the data may preclude a definite comparison, the regression for $\varepsilon = 0.255$, where the convective contributions are strongest, clearly shares the parameter dependencies for the most significant and relevant parameters R/L_n and q with the the simulated one (eq. 4). The experimental shear s was not included in these regressions because of the unavailability of suitably constrained equilibrium reconstructions in this dataset. As q and s are correlated, the larger coefficent for q in eq.(7) may simply account for the contribution of s. The best 5-parameter global regression, which can be compared to eq.(5) is shown in fig.5 and corresponds to the scaling expression

$$R/L_\omega \approx 1.2(t_i^*-\Gamma_N^*) + 0.41R/L_n + 12\varepsilon^{1/2} + 0.41q - 1.9T_i/T_e - 1.7 \quad (8)$$

with $\sigma = 1.29$, $STS = [18, 5.8, 8.2, 3.5, 3.1, 1.9]$ and $STR = [0.52, 0.2, 0.28, 0.09, 0.08, 0]$;

The diffusive component remains the most significant and relevant one, with STR = 0.52, meaning that overall about half of the variation of R/L_ω in the dataset can be attributed to diffusion, with the remainder to be attributed to non-diffusive processes. While there is a strong dependence on $\varepsilon^{1/2}$, corresponding to STR = 0.28, the coefficients for R/L_n, q and T_i/T_e remain similar to the ones

in the local fits (Eq. 6 & 7), suggesting that the inclusion of $\varepsilon^{1/2}$ in the global regression does not significantly bias the dependencies found in the fits for fixed values of ε. No scaling was found with ρ*, nor is any indicated for the pinch by theory, suggesting that the above scaling may hold for ITER.

A direct, point-by-point comparison of theoretically expected angular frequency gradients and observed ones is shown in fig. 6. The expected values were obtained from eq.(2), by using the Prandtl and pinch numbers from GKW, together with the net dimensionless torque from the experiment. As noted before, they fall about 30% short of the observed values, on average.

4. POSSIBLE CONTRIBUTIONS FROM RESIDUAL STRESSES

The systematic differences between GKW and experimental data raise the question whether all or part of the difference may be made up by residual stresses (see ref. [2] for a review). The relative prevalence of the stresses versus pinch depends on the ordering parameter $O_{rs} = \rho_i^*(R/L_{Ti})^2/u$. For $O_{rs} \ll 1$, the pinch is expected to dominate over residual stresses. (Note that in [5] O_{rs} was overestimated by a factor 1.4). Evaluating the contribution of stresses is a challenge for the JET H-mode dataset where $u > 0.1$ in most conditions, even at the pedestal. For the above experimental data, the dimensionless torque was obtained using the NBI deposition code PENCIL [15], which does not include ion orbit effects. Only an adhoc correction was applied to the PENCIL heat flux and torque profiles, based on 10 simulations using the orbit code ASCOT [16], as described in ref. [5]. In order to enable an improved assessment of possible stress contributions, a subset of 150 shots was reprocessed with constrained EFIT calculations (using polarimetry, allowing for non-zero edge pressure and non-zero edge current), followed by ASCOT calculations of torque and heat deposition for each individual sample.

For $\varepsilon < 0.2$ all samples have $O_{rs} < 0.2$ and for more tan 95% of samples $O_{rs} < 0.1$. Only for $\varepsilon > 0.2$, i.e. the two outermost positions, is there a minority of samples with $O_{rs} > 0.2$, the largest value in the dataset being 0.8. Hence significant RS contributions may be expected, for a minority of samples, only at the two positions closest to the edge. Whilst attempts at direct three parameter regressions of eq.(2) including u have so far been unsuccessful, a regression of the form

$$R/L_\omega = \chi_\phi/\chi_i\,(t_i^* - \Gamma_N^*) + RV/\chi_\phi + c_{rs}O_{rs} \qquad (9)$$

shows a clear positive dependence of R/L_ω on O_{rs} at the two outermost positions (and none further inside), as seen for ε=0.255 in fig.7. From the vertical distance of two lines we infer that for the highest values of O_{rs} in the dataset (red stars, $0.6 < O_{rs} < 0.8$) the contribution to R/L_ω that may be associated with residual stresses is as large as the one purely attributed to the pinch, obtained for the limit $O_{rs} \to 0$ and $t_i^* - \Gamma_N^* \to 0$. This is a strong indication, albeit not proof, that residual stresses may contribute to the momentum transport near the edge. Representative profiles of transport coefficients based on these regressions are shown in fig.8. The vertical bars correspond to 90% confidence intervals. For each position the typical stress contribution was evaluated for the average value of O_{rs} at that position as $c_{rs}\,O_{rs}$.

The improved experimental dataset was used as input for a new series of more realistic, electromagnetic, collisional linear GKW simulations using the geometry from the equilibrium reconstruction. Three simulations per sample were performed in order to also determine the up/down asymetry residual stress [17], which is the only one included at the time of writing. The results for the Prandtl number and the pinch are very similar however than those described above. The dominant instability is again found to be an ITG mode. In about 20% of the cases at $k_\theta\rho = 0.15$ and 10% at $k_\theta\rho=0.45$ the most unstable mode was a micro-tearing mode. These modes tend to appear at small minor radii and are only slightly more unstable than the ITG mode, as indicated by the long beating phase before time convergence is reached in the simulations. Linear micro-tearing modes lead to an unrealistically large electron to ion heat flux ratio (from 50 up to several hundreds) and are therefore discarded.

Overall, the results for the pinch and the Prandtl number for ITG unstable samples remain similar to those of the first round of simulations described above, indicating that the cause of the 30% discrepancy with experiment is not to be found in the additional physics so far explored in the second round (fig.9). The scatter of the results is however larger, possibly as a result of uncertainties associated with the additional input parameters. As expected, the up/down asymetry RS is perceptible only at the two outermost positions. At $\varepsilon = 0.255$ the residual stress contributes only about 0.7 to R/L_ω for $k_\theta\rho = 0.15$. The contribution for $k_\theta\rho = 0.45$ is negative, suggesting that the net, spectrum-averaged, contribution would be lower still. Clearly a proper spectral average is required and other residual stress contributions need to be evaluated, in particular the one resulting from $E\times B$ shearing. Even though further stress contributions may be found near the edge, it seems questionable that residual stresses may account for the difference between the experimental convection number and the GKW pinch further in the core $(\varepsilon<0.2)$.

DISCUSSION AND CONCLUSIONS

The analysis of the JET database, together with extensive linear gyrokinetic calculations show that the bulk of the non-diffusive momentum transport in rotating JET H-modes can be attributed to the Coriolis pinch. This is supported by similar parameter scalings of the observed convection with those of the predicted pinch. No scaling was found with ρ^*, nor is any indicated for the pinch by theory, suggesting that the experimental scaling may hold for the pinch in ITER. The fact that the theoretical pinch underpredicts the observed convection by typically 30% is so far not understood. Possible reasons may include misestimates of spectral averages from only two wavenumbers, differences between linear and non-linear saturated transport coefficients, differential neoclassical rotation of deuterium and carbon as measured by charge exchange spectroscopy and the contribution of residual stresses. While there is evidence for residual stresses near the edge, it is questionable whether residual stresses can explain the difference in the core, where the ordering parameter O_{rs} is below 0.1 in most cases.

ACKNOWLEDGEMENTS

The calculations for this work were performed using HPC resources from GENCI-CCRT/IDRIS (Grant 2012-100182). This work was supported by EURATOM and carried out within the framework of the European Fusion Development Agreement. The views and opinions expressed herein do not necessarily reflect those of the European Commission.

REFERENCES

[1]. C. Angioni et al, Nuclear Fusion special issue: 13th International Workshop on H-mode Physics and Transport Barriers, Oxford, October 2011, to be published, (2012)
[2]. A.G. Peeters et al, Nuclear Fusion, **51**, 094027 (2011)
[3]. M.Yoshida et al. Nuclear Fusion **52** (2012) 023024
[4]. W.M. Solomon et al, Nuclear Fusion 51 (2011) 073010
[5]. H. Weisen et al, Nuclear Fusion special issue: 13th International Workshop on H-mode Physics and Transport Barriers, Oxford, October 2011, to be published, (2012)
[6]. T. Tala et al, Physical Review Letters **102**, 075001 (2009)
[7]. T. Tala et al, Nuclear Fusion **51**, 123002 (2011)
[8]. P.C. de Vries et al, Nuclear Fusion **48**, 035007 (2008)
[9]. A. G. Peeters et al., Computer Physics Communications, **180**, (2009) 2650
[10]. Y. Camenen et al., Nuclear Fusion **51**, 073039 (2011)
[11]. A.G. Peeters et al, Physics of Plasmas **16**, 062311 (2009)
[12]. N. Kluy et al, Physics of Plasmas **16**, 122302 (2009)
[13]. A.G. Peeters et al, Physical Review Letters **98**, 265003 (2007)
[14]. A.G. Peeters et al, Physics of Plasmas **16**, 062311 (2009)
[15]. C.D. Challis et al, Nuclear Fusion **29**, (1989) 563
[16]. J.A. Heikkinen *et al*., Journal of Computational Physics **173**, (2001) 527
[17]. Y. Camenen et al, Physical Review Letters **102**, (2009) 125001

	$\lvert t_i^* - \Gamma_N^* \rvert$	u	R/L_ω	R/L_n	R/L_{Ti}	R/L_{Te}	T_i/T_e	ε	ν_{eff}	β	ρ_i^*	q	s
min	0.05	0.05	0.4	1	3	3	0.6	0.075	0.06	0.001	0.001	0.9	0.01
max	14	0.38	24	10	19	17	2.7	0.255	5.2	0.049	0.005	4.6	10

Table 1: Dimensionless parameter ranges in JETPEAK H-mode and hybrid database and across the minor radius from $\rho = 0.25$ *to 0.85. Here* $u = R\omega/v_i = R\omega/(2T_i/m_i)^{1/2}$ *is the Mach number,* $L_\omega = \omega/\nabla\omega$ *etc,* $\varepsilon = r/R$ *is the inverse aspect ratio,* $\nu_{eff} = 10^{-14} R Z_{eff} n_e T_e^{-2}$ *is the normalised collisionality,* β *is the local thermal plasma pressure normalised to the magnetic pressure,* $\rho_i^* = (2T_i/m_i)^{1/2}/(\omega_{ci} R)$ *is the thermal ion Larmor radius normalised to R, q is the local safety factor obtained using the equilibrium code EFIT and* $s = \varepsilon R/L_q$.

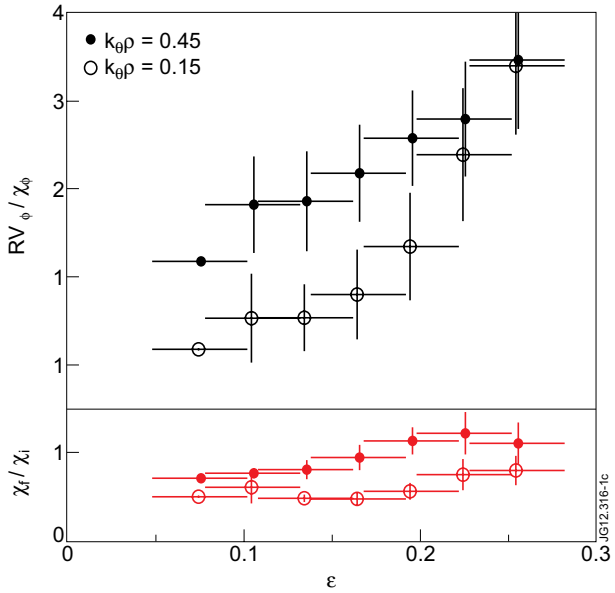

Figure 1: Average and standard deviation (bars) of Prandtl (red) and pinch numbers (black) from GKW, for two different wavenumbers.

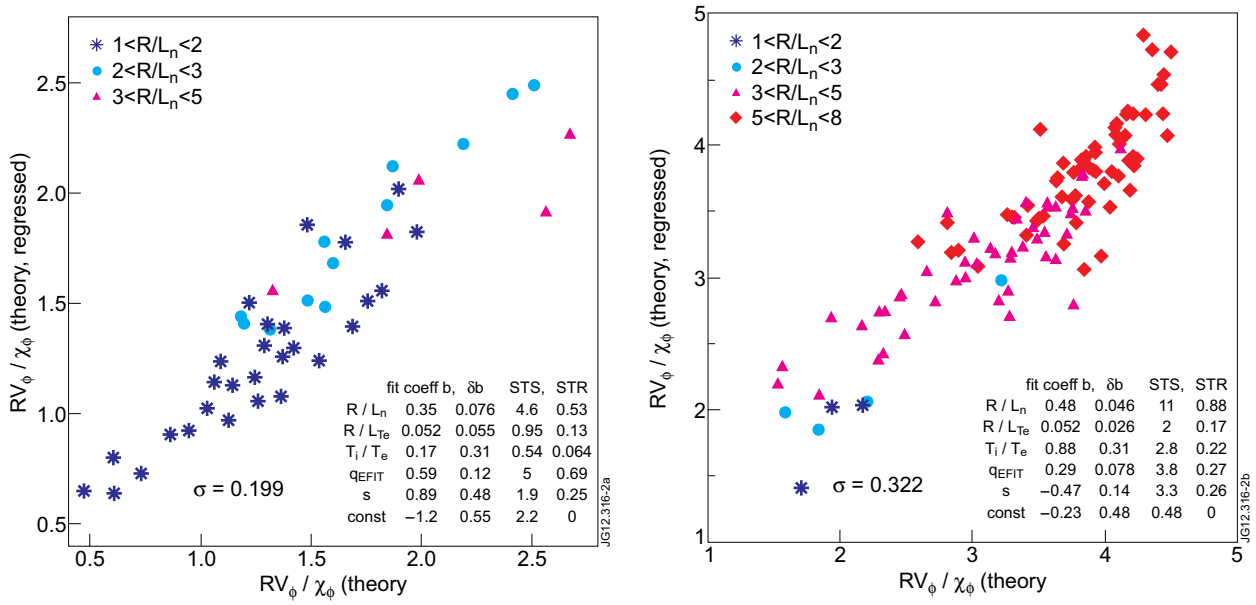

Figure 2: Regressions for the theoretical Coriolis pinch number. a) Left: ε = 0.165 (mid-radius) and b) Right: ε = 0.255 (near the edge). The symbols refer to the normalized density gradient R/L_n.

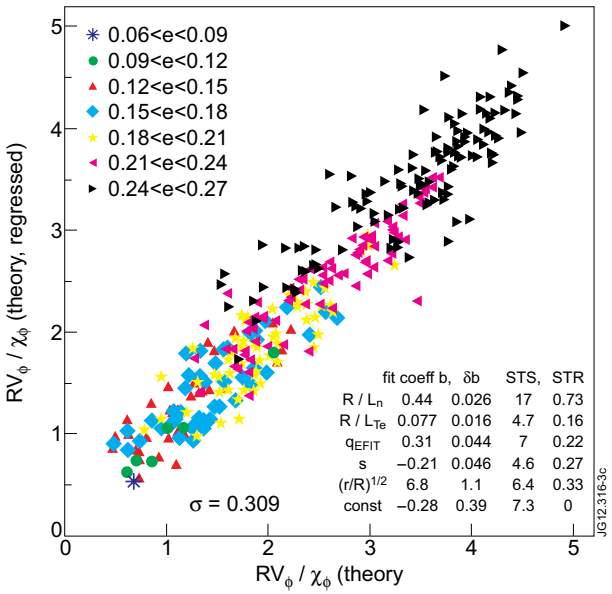

Figure 3: Best global 5-parameter regressions for the theoretical Coriolis pinch number.

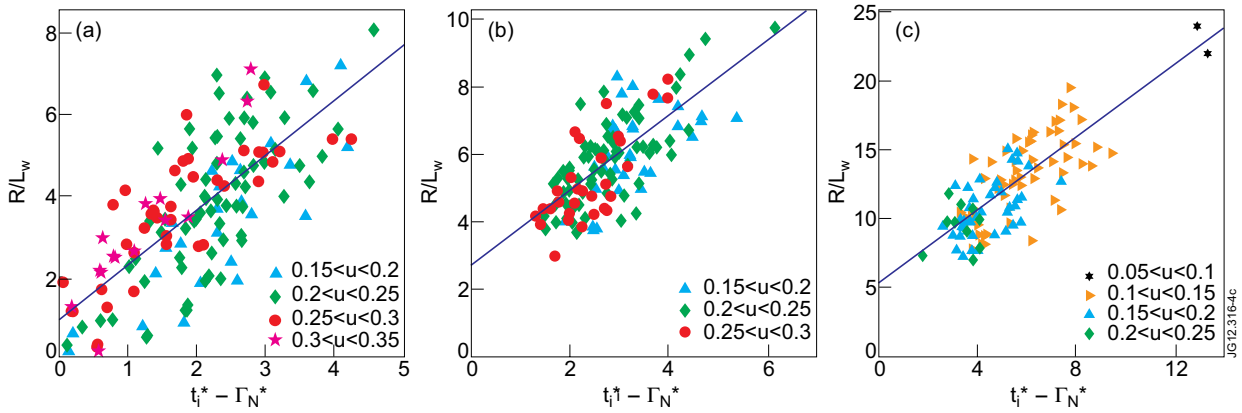

Figure 4: Fits of eq.(2) for experimental data, showing a diffusive component (slope) and a non-diffusive component (intercept at zero effective torque) for three positions, a) $\varepsilon \approx 0.075$ ($r/a \approx 0.25$) b) $\varepsilon \approx 0.165$ ($r/a \approx 0.55$) and c) $\varepsilon \approx 0.255$ ($r/a \approx 0.85$). The symbols refer to classes of Mach number u. The Prandtl number is obtained as the inverse of the slope of the regressed line.

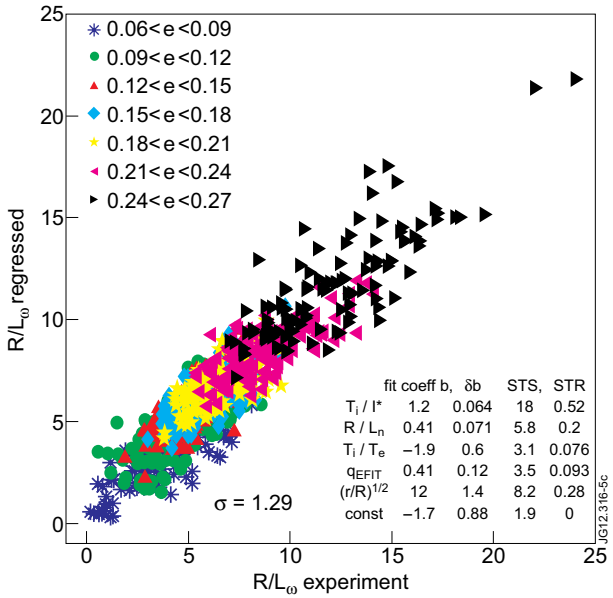

Figure 5: Global regression on experimental data.

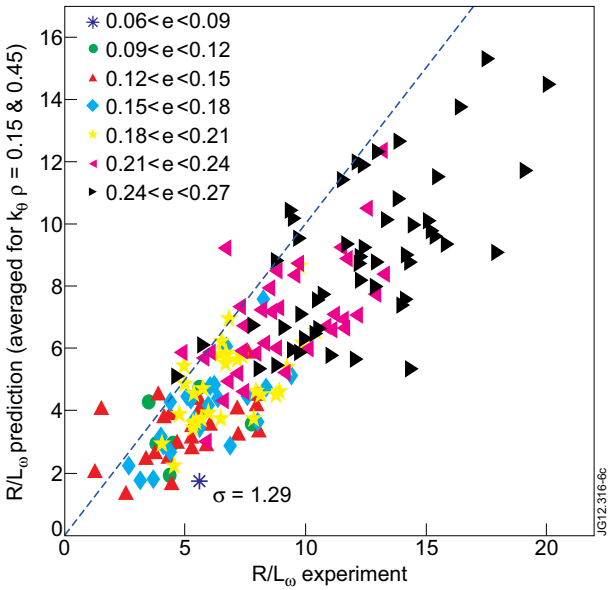

Figure 6: Sample-by-sample comparison of experimental and modeled R/L_ω

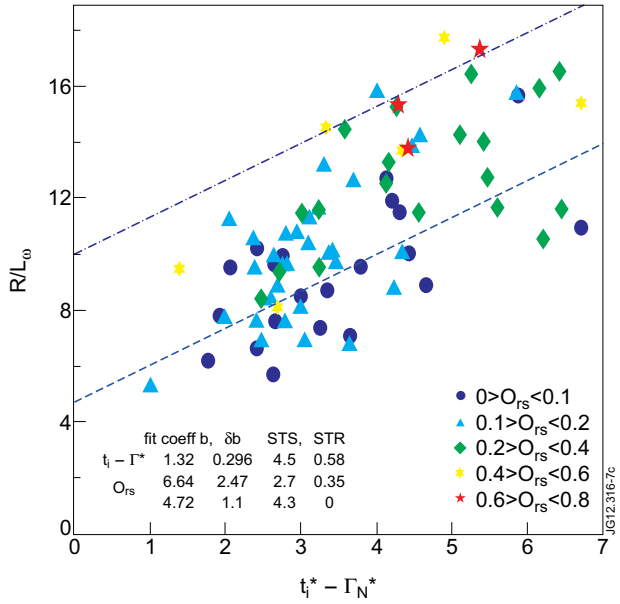

Figure 7: Three parameter fit of experimental data at ε = 0.255, with lines corresponding to O_{rs} = 0 (lower) and O_{rs} = 0.8. The latter corresponds to the largest value for O_{rs} in the set.

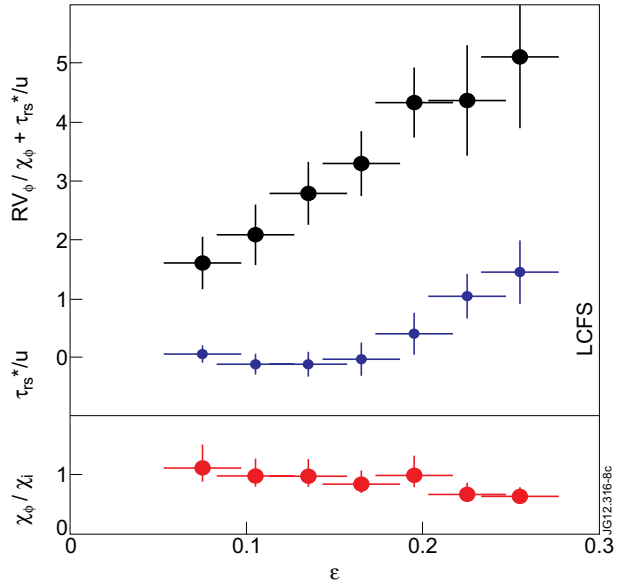

Figure 8: Representative profiles of momentum transport parameters from experiment. Horizontal bars represent range over which gradients were evaluated. Vertical bars are 90% confidence intervals of three parameter fit over whole dataset.

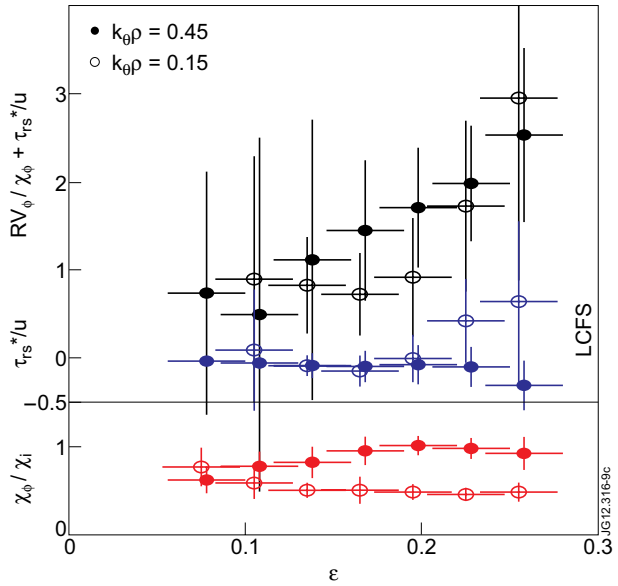

Figure 9: Profiles of momentum transport parameters from linear, electromagnetic, collisional GKW simulations in realistic geometry. The residual stress contribution to R/L_ω shown here (blue symbols) only includes the up-down asymmetry stress.